OPTICS CONTINUUM

Double-pass second-harmonic generation of picosecond pulses with custom-poled KTP crystal

YUMIN ZHANG,[1] JUN LIU,[1] ZHONGZHONG QIN,[1,2] AND XIAOLONG SU[1,2,*]

[1]State Key Laboratory of Quantum Optics and Quantum Optics Devices, Institute of Opto-Electronics, Shanxi University, Taiyuan, 030006, China
[2]Collaborative Innovation Center of Extreme Optics, Shanxi University, Taiyuan, Shanxi 030006, China
*suxl@sxu.edu.cn

Abstract: We present the double-pass second-harmonic generation (SHG) of picosecond pulses with a custom-poled potassium titanyl phosphate (KTP) nonlinear crystal. The average output power of 466 mW at central wavelength of 515.7 nm is obtained with the input of 1.2 W fundamental laser pulses. Compared to the highest conversion efficiency of 29.1% in the single-pass SHG, the conversion efficiency in the double-pass SHG is increased to 38.8%. Moreover, the average RMS stability of 0.67% in 2 hours and high beam quality ($M^2 < 1.10$) of the second-harmonic pulses is observed. The presented results provide an efficient method to enhance the conversion efficiency of SHG for picosecond pulses.

1. Introduction

Picosecond pulses with high peak power and narrow pulse width has broad applications, such as material processing [1,2], laser ranging [3,4], coherent anti-Stokes Raman imaging [5,6] and stimulated Raman scattering imaging [7–10]. Notably, quantum-enhanced stimulated Raman scattering microscopy that employs picosecond pulsed squeezed state as probe source presents the enhancement of 1.3 dB signal-to-noise ratio of imaging [11]. To prepare a picosecond pulsed squeezed state, the pump pulses of the parametric down conversion is obtained through the second-harmonic generation (SHG) of the fundamental picosecond pulses.

The conversion efficiency of the SHG is an important parameter, which determines the output power of the SHG [12]. There are several parameters affect the conversion efficiency of SHG, such as the second-order nonlinear coefficient of the crystal, the power density of the input fundamental frequency light, the time that the fundamental laser pass through the crytal. Therefore, using a longer nonlinear crystal or allowing the laser to pass through the crystal more times can increase the conversion efficiency of SHG if the input power of the fundamental laser is fixed.

Two methods have been developed to increase the number of times that the fundamental laser pass through the crystal, which are the double-pass SHG and resonant cavity. In the double-pass scheme, the fundamental pump laser is focused into the nonlinear crystal two times. An impressive conversion efficiency of 60% was obtained with double-pass SHG for the continuous-wave laser, which is more than twice as high as the efficiency of the single-pass geometry [13]. In the SHG with resonant cavity, which greatly increase the laser intensity in cavity, an conversion efficiency of 75% using a periodically poled potassium titanyl phosphate (PPKTP) crystal in the ring cavity [14] and an conversion efficiency of 87% using an lithium-triborate (LBO) crystal within a F-P cavity has been reported [15] for the continuous-wave laser. While in the SHG of pulse laser, the common approach for generating second-harmonic of picosecond pulses is passing the pulses through a crystal once, i.e., single-pass SHG. The conversion efficiencies of 41% [16] and 40% [17] were reached with PPKTP crystals in the single-pass SHG of picosecond pulses. Although

#519697 https://doi.org/10.1364/OPTCON.519697
Journal © 2024 Received 23 Jan 2024; revised 3 Mar 2024; accepted 4 Mar 2024; published 13 Mar 2024

OPTICS CONTINUUM

the technology of double-pass SHG has been applied to improve the conversion efficiency for continuous-wave [13] and low repetition rate picosecond laser [18], it has not been reported for the high repetition rate picosecond laser.

In this work, we present SHG of picosecond pulses with a custom-poled KTP crystal working in both single-pass and double-pass configurations. The double-pass SHG is realized by applying a concave mirror to reflect both the fundamental pulses with central wavelength of 1031.3 nm and second-harmonic pulses with central wavelength of 515.7 nm generated in the single-pass SHG. Based on the measured output power of the second-harmonic pulses in the single-pass and double-pass SHG respectively, we show that the maximum conversion efficiency of 29.1% in single-pass SHG is improved to 38.8% in double-pass SHG at fundmental power of 1.2 W. We also investigate power stability and beam profile of the SHG. Our results demonstrate the advantage of double-pass SHG in increasing the conversion efficiency of SHG for picosecond pulses.

2. Experimental setup

The schematics of the single-pass and double-pass SHG experimental setups are shown in Figs. 1(a) and 1(b), respectively. The laser employed in this work is a picosecond pulsed laser (APE picoEmerald), which generates pulses at central wavelength of 1031.3 nm with a repetition frequency of 80 MHz and a pulse duration of 2 ps, corresponding to spectrum width of 0.9 nm. A Faraday isolator (FI) is used to prevent backreflections to the laser. The laser power is adjusted by the combination of the half-wave plate and polarization beam splitter. Another half-wave plate is used to optimize the laser polarization for optimal conversion efficiency of second-harmonic generation, on account of the crystal in the experiment requires input light with vertical polarization. The pulsed laser is focused into the custom-poled KTP crystal using a plano-convex lens with a focal length of 100 mm. The waist radius in the central of the crystal is $\omega_0 = 21.9\ \mu m$, corresponding to a loose Boyd-Kleinman parameter $\xi = L/b = 0.37$ [12]. Here $L = 2$ mm is the crystal length and $b = 2\pi\omega_0^2 n_1/\lambda$ is the confocal parameter, where n_1 is the refractive index of the fundamental wave in the crystal and λ is the fundamental wavelength.

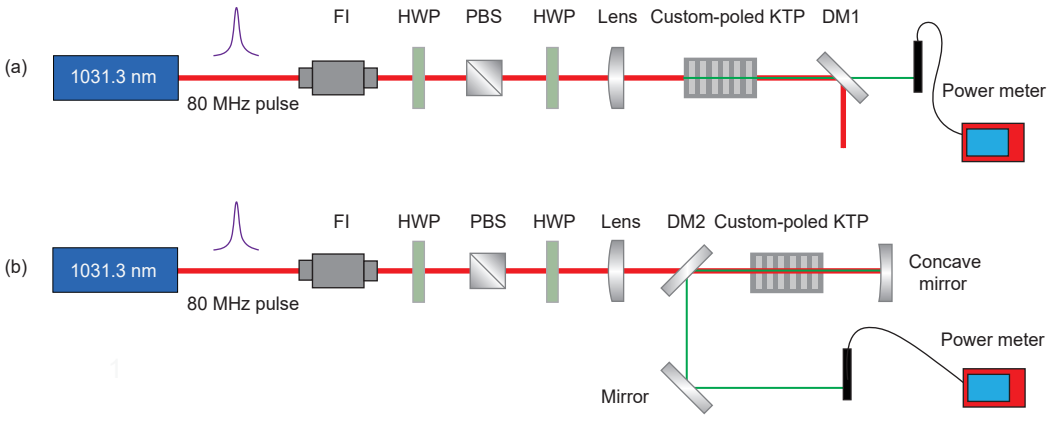

Fig. 1. (a) Experimental setup of the single-pass SHG with a custom-poled KTP crystal for a picosecond pulsed laser. (b) Experimental setup of the double-pass SHG. FI, Faraday isolator; HWP: half-wave plate; PBS: polarizing beam splitter; KTP: potassium titanyl phosphate crystal; DM: Dichroic mirror.

In our SHG system, a 2 mm long custom-poled KTP crystal (ordered from Raicol) with a fixed domain width of 8.1 μm is used. We obtain the Gaussian-shaped phase matching of the crystal by customizing the polarization configuration and directly manipulating the direction of the

OPTICS CONTINUUM

domains in the grating, while keeping the width of each domain fixed [19]. The high nonlinear coefficients [14,20,21] and the low phase matching temperature make the crystal suitable for our system. On the other hand, using a longer crystal would actually be a better choice by taking into account the duration of the pulse and the group velocity mismatch between the fundamental and second-harmonic pulses [22–24]. The crystal is placed inside a homemade oven, equipped with a thermocouple and Peltier element for precise temperature control. In addition, an external shield is used to prevent thermal exchange between the oven and its surroundings, ensuring the temperature stability of crystal better than 0.01 $^{\circ}C$.

In the single-pass experiment, as shown in Fig. 1(a), the power meter is placed after a dichroic mirror (CVI Laser Optics, BSR-15-1025) with reflectivity of 96.3% at 1031.3 nm and transmissivity of 97.2% at 515.7 nm to filter out the fundamental pulses. In this case, the power measured by the power meter represents the power of the single-pass frequency-doubled light.

In the double-pass SHG experiment, as shown in Fig. 1(b), to make the pulses pass through the crystal for a second time, the laser beam is reflected by a silver-coated concave mirror (Daheng optics, GCC-102224) with a focal length of 100 mm. It is important to make sure that the concave mirror is precisely positioned to achieve perfect alignment of the foci of the first and the second pass. Otherwise, the conversion efficiency of double-pass SHG is decreased. Ultimately, the second-harmonic pulses is separated using a dichroic mirror (Semrock, FF980) with a reflectivity of 97.0% at 515.7 nm and a transmissivity of 96.6% at 1031.3 nm. The power meter is placed behind the mirror to measure the power of the double-pass second-harmonic pulses.

3. Experimental results and discussion

The dependence of second-harmonic output power for both single-pass and double-pass SHG on the fundamental power is shown in Fig. 2, where the optimum temperature of the KTP crystal in single-pass and double-pass SHG is applied, respectively. At low fundamental power levels, the second-harmonic power increases quadratically with the fundamental power. However, at higher power levels, they exhibit a linear relationship due to pump depletion [25]. To avoid the presence of damage in the crystal, the maximum fundamental power is set to 1.2 W. Under this condition, the maximum output power of 349 mW and 466 mW is observed in the single-pass and double-pass SHG, respectively.

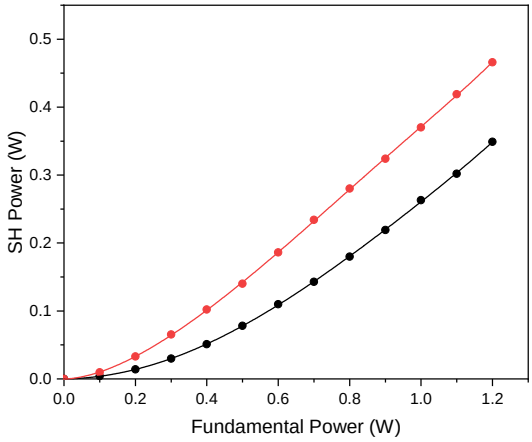

Fig. 2. The measured second-harmonic output powers as a function of fundamental power. The black and red dots represent the single-pass and double-pass SHG, respectively.

Figure 3 shows the conversion efficiency of both single-pass and double-pass SHG as a function of fundamental powers. In the single-pass SHG, a maximum conversion efficiency of

OPTICS CONTINUUM

29.1% is achieved at a fundamental power of 1.2 W. In contrast to that, the double-pass SHG achieves a higher maximum conversion efficiency of 38.8% at the same fundamental power. With the fundamental power of 1.2 W, a 1.34 times improvement has been observed through the double-pass SHG.

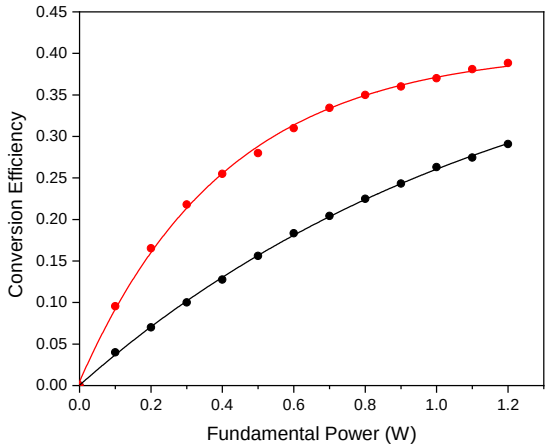

Fig. 3. The conversion efficiency of SHG as a function of fundamental power. The black and red dots represent the conversion efficiency of single-pass and double-pass SHG scheme, respectively.

Figure 4 shows the fluctuation of second-harmonic power in the single-pass SHG and double-pass SHG. With a 2-hour observation period and a 900 mW fundamental laser, the second-harmonic pulses in single-pass and double-pass show peak-to-peak fluctuations of 0.99% and 3.34% and standard deviations of 0.23% and 0.67%, respectively.

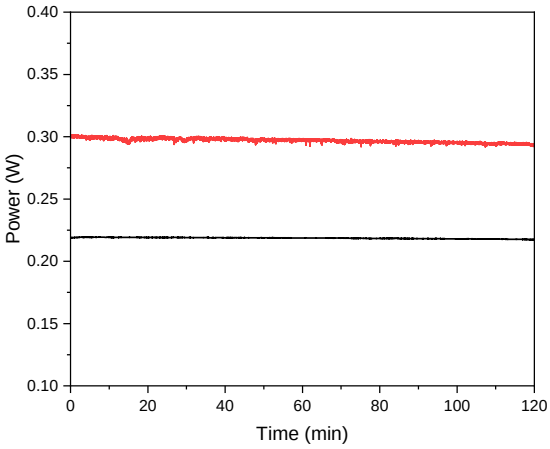

Fig. 4. The power stability of the second-harmonic generation. The black and red curves are the measured power in the single-pass and double-pass SHG, respectively.

We also characterize the beam profile of the second-harmonic pulses in double-pass SHG by measuring the M^2 factor. The value of the M^2 factor is fitted by measuring a range of beam sizes with optical beam profiles (Thorlabs, BP209) near the waist. As shown in Fig. 5, the M^2 value is 1.10 in both the horizontal and vertical directions. Additionally, the insert shows the beam profile at the waist position, which has an ellipticity of 99.32%.

OPTICS CONTINUUM

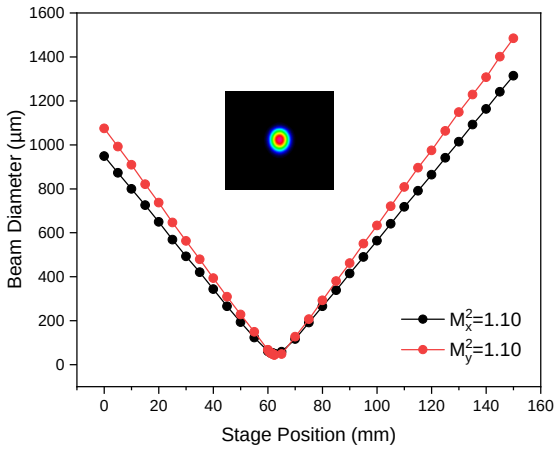

Fig. 5. The M^2 factor measurement result of the double-pass second-harmonic generation scheme. Inset: corresponding beam profile. The M^2 value is 1.10 in both the horizontal and vertical directions.

The measured pulse widths of the fundamental pulses and the second-harmonic pulses are shown in Fig. 6. For an ideal SHG process, the pulse width of the second-harmonic pulses will be shortened due to nonuniform intensity distribution of fundamental pulses [26]. However, considering the group velocity mismatch between fundamental pulses and harmonic pulses, the pulse width will be broaden. In our experiment, the group velocity mismatch between 515.7 nm and 1031.3 nm is calculated to 6.8 ps/cm [27]. According to the time walk-off length of the crystal $L_T = \tau_p/\beta$, where τ_p is the pulse width of the fundamental wave and β is the GVM parameter between the pump and the SHG pulse, it would be helpful to use a crystal length of at least 3 mm. Therefore, in the single-pass SHG configuration with the crystal length of 2 mm, the pulse width of harmonic wave shorten from 2.07 ps to 1.67 ps. However, in the double-pass SHG configuration, the total 4 mm length crystal leads to 2.7 ps walk-off, making the pulse width broaden from 1.67 ps to 1.87 ps.

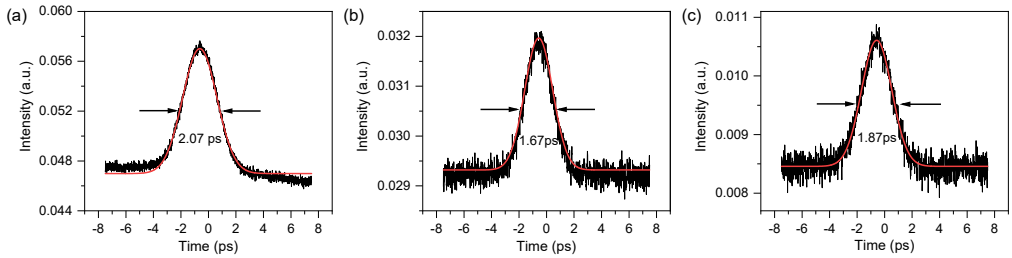

Fig. 6. The measured pulse widths of the fundamental pulses (a) and second-harmonic pulses of the single-pass (b) and double-pass configuration (c), respectively.

As we know, the conversion efficiency of SHG is proportional to the square of the crystal length at low fundamental power level [26]. In principle, the theoretical conversion efficiency of the double-pass scheme can be enhanced to four times of that of the single-pass scheme in the mW regime [28] and low W regime [29]. The possible elements that affect the conversion efficiency are as following. Firstly, the loss of fundamental light during the first pass and the imperfect matching conditions of the second pass resulted in discrepancies between the experimental results and theoretical expectations in reality. Secondly, the 0.72 nm acceptable bandwidth of

OPTICS CONTINUUM

our custom-pole KTP crystal [30,31] also leads to the decrease of SHG efficiency. Thirdly, The Boyd-Kleinman parameter of 0.37 is relatively small compared to the optimal focus factor of 2.84. Moreover, the conversion efficiency of the SHG process can be further improved by using crystal and concave mirror with coatings specifically designed for the fundamental and second-harmonic wavelengths.

4. Conclusion

In conclusion, we experimentally demonstrate the double-pass SHG of picosecond pulse with a custom-poled KTP crystal. Compared to the single-pass SHG, the conversion efficiency of double-pass SHG is improved from 29.1% to 38.8% with 1.2 W input fundamental pulses, which corresponds to 1.34 times of enhancement. The excellent beam quality and power stability of the second-harmonic pulses makes it suitable for further applications, such as the pump light for the preparation of squeezed light of picosecond pulse.

Funding. National Natural Science Foundation of China (11834010); Fundamental Research Program of Shanxi Province (20210302121002, 20210302122002); the Fund for Shanxi 1331 Project Key Subjects Construction.

Disclosures. The authors declare that there are no conflicts of interest related to this article.

Data availability. Data underlying the results presented in this paper are not publicly available at this time but may be obtained from the authors upon reasonable request.

References

1. K. Sugioka and Y. Cheng, "Ultrafast lasers–reliable tools for advanced materials processing," Light: Sci. Appl. **3**(4), e149 (2014).
2. K. Cvecek, F. Stenglein, I. Miyamoto, *et al.*, "Influence of wavelength on glass welding by ultra-short laser pulses," J. Laser Micro/Nanoeng. **12**(2), 115–119 (2017).
3. G. Bury, K. Sośnica, and R. Zajdel, "Multi-GNSS orbit determination using satellite laser ranging," J. Geod. **93**(12), 2447–2463 (2019).
4. B. D. Loomis, K. E. Rachlin, D. N. Wiese, *et al.*, "Replacing GRACE/GRACE–FO C_{30} with satellite laser ranging: impacts on Antarctic ice sheet mass change," Geophys. Res. Lett. **47**, (2020).
5. C. L. Evans and X. S. Xie, "Coherent anti-stokes Raman scattering microscopy: chemical imaging for biology and medicine," Annual Rev. Anal. Chem. **1**(1), 883–909 (2008).
6. C. H. Camp Jr, Y. J. Lee, J. M. Heddleston, *et al.*, "High-speed coherent Raman fingerprint imaging of biological tissues," Nat. Photonics **8**(8), 627–634 (2014).
7. C. W. Freudiger, W. Min, B. G. Saar, *et al.*, "Label-free biomedical imaging with high sensitivity by stimulated Raman scattering microscopy," Science **322**(5909), 1857–1861 (2008).
8. C. W. Freudiger, W. Yang, G. R. Holtom, *et al.*, "Stimulated Raman scattering microscopy with a robust fibre laser source," Nat. Photonics **8**(2), 153–159 (2014).
9. M. Ji, S. Lewis, S. Camelo-Piragua, *et al.*, "Detection of human brain tumor infiltration with quantitative stimulated Raman scattering microscopy," Sci. Transl. Med. **7**(309), 309ra163 (2015).
10. F. Lu, D. Calligaris, O. I. Olubiyi, *et al.*, "Label-free neurosurgical pathology with stimulated Raman imaging," Cancer Res. **76**(12), 3451–3462 (2016).
11. C. A. Casacio, L. S. Madsen, A. Terrasson, *et al.*, "Quantum-enhanced nonlinear microscopy," Nature **594**(7862), 201–206 (2021).
12. G. D. Boyd and D. A. Kleinman, "Parametric interaction of focused Gaussian light beams," J. Appl. Phys. **39**(8), 3597–3639 (1968).
13. M. Stappel, D. Kolbe, and J. Walz, "Continuous-wave, double-pass second-harmonic generation with 60% efficiency in a single MgO:PPSLT crystal," Opt. Lett. **39**(10), 2951 (2014).
14. R. L. Targat, J.-J. Zondy, and P. Lemonde, "75%-Efficiency blue generation from an intracavity PPKTP frequency doubler," Opt. Commun. **247**(4-6), 471–481 (2005).
15. C. H. Feng, S. Vidal, P. Robert, *et al.*, "High power continuous laser at 461 nm based on a compact and high-efficiency frequency-doubling linear cavity," Opt. Express **29**(17), 27760 (2021).
16. T. Hirano, K. Kotani, T. Ishibashi, *et al.*, "3 dB squeezing by single-pass parametric amplification in a periodically poled $KTiOPO_4$ crystal," Opt. Lett. **30**(13), 1722 (2005).
17. Y. Zhang, T. Furuta, R. Okubo, *et al.*, "Experimental generation of broadband quadrature entanglement using laser pulses," Phys. Rev. A **76**(1), 012314 (2007).
18. J. Huang, H. Lin, C. Guo, *et al.*, "Enhanced cascaded up-conversion from periodically poled lithium niobate in a double-pass configuration," Infrared Phys. Technol. **124**, 104206 (2022).
19. A. Dosseva, Ł. Cincio, and A. M. Brańczyk, "Shaping the joint spectrum of down-converted photons through optimized custom poling," Phys. Rev. A **93**(1), 013801 (2016).

OPTICS CONTINUUM

20. G. R. Fayaz, M. Ghotbi, and M. Ebrahim-Zadeh, "Efficient second-harmonic generation of tunable femtosecond pulses into the blue in periodically poled KTP," Appl. Phys. Lett. **86**(6), 061110 (2005).
21. M. Leonardi, M. Bazzan, L. Conti, *et al.*, "Efficient second harmonic generation with compact design: double-pass and cavity configurations," Laser Phys. **28**(11), 115401 (2018).
22. S. Wang, V. Pasiskevicius, and F. Laurell, "Ultraviolet generation by first-order frequency doubling in periodically poled $KTiOPO_4$," Opt. Lett. **23**(24), 1883–1885 (1998).
23. H. Zhong, L. Zhang, Y. Li, *et al.*, "Group velocity mismatch-absent nonlinear frequency conversions for mid-infrared femtosecond pulses generation," Sci. Rep. **5**(1), 10887 (2015).
24. M. Galletti, H. Pires, V. Hariton, *et al.*, "High efficiency second harmonic generation of nanojoule-level femtosecond pulses in the visible based on BiBO," High Power Laser Sci. Eng. **7**, e11 (2019).
25. S. C. Kumar, G. K. Samanta, and M. Ebrahim-Zadeh, "High-power, single-frequency, continuous-wave second-harmonic-generation of ytterbium fiber laser in PPKTP and MgO:sPPLT," Opt. Express **17**(16), 13711–13726 (2009).
26. J. Yao and Y. Wang, "*Nonlinear Optics and Solid-State Lasers: Advanced Concepts, Tuning-Fundamentals and Applications*," (Springer, Berlin, Heidelberg.) 164, 125–177 (2012).
27. K. Hayata and M. Koshiba, "Group-velocity-matched second-harmonic generation: An efficient scheme for femtosecond ultraviolet pulse generation in periodically domain-inverted β-BaB_2O_4," Appl. Phys. Lett. **62**(18), 2188–2190 (1993).
28. G. Imeshev, M. Proctor, and M. M. Fejer, "Phase correction in double-pass quasi-phase-matched second-harmonic generation with a wedged crystal," Opt. Lett. **23**(3), 165–167 (1998).
29. S. Spiekermann, F. Laurell, V. Pasiskevicius, *et al.*, "Optimizing non-resonant frequency conversion in periodically poled media," Appl. Phys. B **79**(2), 211–219 (2004).
30. S. Emanueli and A. Arie, "Temperature-dependent dispersion equations for $KTiOPO_4$ and $KTiOAsO_4$," Appl. Opt. **42**(33), 6661–6665 (2003).
31. J. L. Tambasco, A. Boes, L. G. Helt, *et al.*, "Domain engineering algorithm for practical and effective photon sources," Opt. Express **24**(17), 19616–19626 (2016).